Volume 14
Number 9
7 March 2023
Pages 2249–2470

Chemical Science

rsc.li/chemical-science

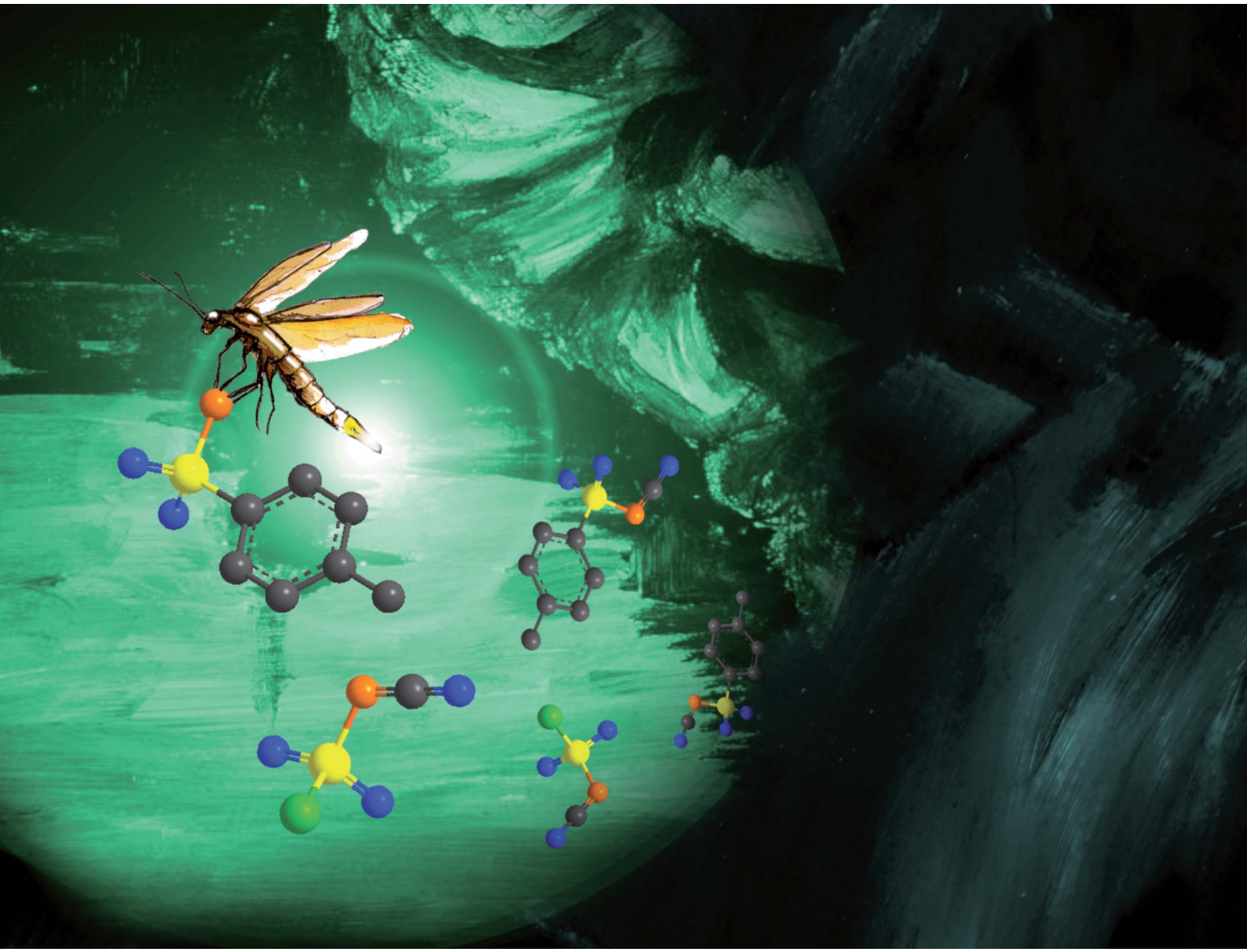

ISSN 2041-6539

ROYAL SOCIETY OF CHEMISTRY

EDGE ARTICLE

Cristian A. Strassert, Evamarie Hey-Hawkins *et al.*
Facile modification of phosphole-based aggregation-induced emission luminogens with sulfonyl isocyanates

Chemical Science

ROYAL SOCIETY OF CHEMISTRY

EDGE ARTICLE

View Article Online
View Journal | View Issue

Check for updates

Cite this: *Chem. Sci.*, 2023, **14**, 2267

All publication charges for this article have been paid for by the Royal Society of Chemistry

Received 17th January 2023
Accepted 23rd January 2023

DOI: 10.1039/d3sc00308f

rsc.li/chemical-science

Facile modification of phosphole-based aggregation-induced emission luminogens with sulfonyl isocyanates†

Nils König, [a] Yokari Godínez-Loyola, [b] Fangshun Yang, [c] Christian Laube, [c] Michael Laue, [d] Peter Lönnecke, [a] Cristian A. Strassert *[b] and Evamarie Hey-Hawkins *[a]

Phosphole oxides undergo a highly chemoselective reaction with sulfonyl isocyanates forming sulfonylimino phospholes in high yields. This facile modification proved to be a powerful tool for obtaining new phosphole-based aggregation-induced emission (AIE) luminogens with high fluorescence quantum yields in the solid state. Changing the chemical environment of the phosphorus atom of the phosphole framework results in a significant shift of the fluorescence maximum to longer wavelengths.

Introduction

Since Tang *et al.* first described the principle of aggregation-induced emission (AIE) for methylpentaphenylsilole about 20 years ago,[1] the interest and importance of this research area have steadily increased, as indicated by the number of publications per year.[2,3] The potential applications of AIE range from bioanalytics[4–6] and materials science[7] to optoelectronics.[8] AIE describes the phenomenon of molecules that show minimal or no emission in solutions but significantly increased emission in the solid or aggregated state.[9]

These molecular properties, especially in rotovibration mode-rich compounds, can be well explained by the structural characteristics of a molecule. Thus, it was noted that in AIE luminogens (AIEgens) in the excited state, the non-radiative decay is accelerated by intramolecular motions.[13] These types of intramolecular rotations are strongly restricted in the aggregated state, mainly by intermolecular C_{aryl}–H$\cdots\pi$ interactions, which leads to an enhancement of luminescence.[14] This effect is clearly demonstrated in phenyl-rich systems shown in Fig. 1. In diluted solutions, low photoluminescence quantum yields were observed (Φ_F = 0.1–0.3%),[12,15] due to numerous possibilities for the rotation of the phenyl rings. However, in the solid state, these compounds become strongly luminescent ($\Phi_{F(solid)}$ = 36–78%),[12,15] because of the restriction of intramolecular rotations (RIRs). In addition to the well-known AIEgens of tetraphenylethenes (TPEs),[10] phenylsiloles[11] and phenylpyrazines,[16] the incorporation of the phosphole motif into π-conjugated molecular frameworks and aryl-rich systems received considerable attention.[17–23]

Phospholes are five-membered organophosphorus heterocycles and the phosphorus analogues of pyrroles. Compared to pyrroles and other conjugated five-membered heterocycles, phospholes have much lower aromaticity due to the pyramidal environment at the phosphorus atom.[25] Thus, the orientation of the lone pair of electrons at the P-atom does not favor interaction with the neighboring orbitals of the π system,[26,27] allowing facile modifications.[19] The change in the chemical environment of the phosphorus atom has a major influence on the photophysical properties of the molecule, as demonstrated for dithienyl-phosphole (DTP, Scheme 1). The advantages of

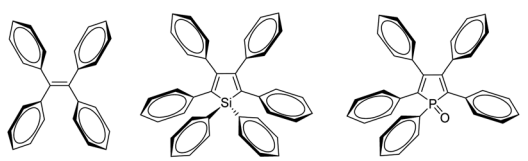

	TPE	HPS	PPPO
Φ_F	0.2 %	0.1 %	0.3 %
Φ_F(solid)	49 %	78 %	36 %

Fig. 1 Molecular structures of AIEgens tetraphenylethene (TPE),[10] hexaphenylsilole (HPS),[11] and pentaphenylphosphole oxide (PPPO)[12] and their fluorescence quantum yields in solution (Φ_F) and the solid state (Φ_F(solid)).

[a]*Leipzig University, Faculty of Chemistry and Mineralogy, Institute of Inorganic Chemistry, Johannisallee 29, 04103 Leipzig, Germany. E-mail: hey@uni-leipzig.de*

[b]*Institut für Anorganische und Analytische Chemie, CiMiC, SoN and CeNTech, Westfälische Wilhelms-Universität Münster, Heisenbergstraße 11, 48149 Münster, Germany. E-mail: cstra_01@uni-muenster.de*

[c]*Leibniz-Institut für Oberflächenmodifizierung e.V., Permoserstrasse 15, 04318 Leipzig, Germany*

[d]*Leipzig University, Faculty of Chemistry and Mineralogy, Institute of Organic Chemistry, Johannisallee 29, 04103 Leipzig, Germany*

† Electronic supplementary information (ESI) available: Methods, synthesis, crystallographic data, compound spectra, optical properties and theoretical calculations. CCDC 2219165–2219173. For ESI and crystallographic data in CIF or other electronic format see DOI: https://doi.org/10.1039/d3sc00308f

Open Access Article. Published on 03 Feabhra 2023. Downloaded on 28/04/2026 00:38:03. This article is licensed under a Creative Commons Attribution-NonCommercial 3.0 Unported Licence.

Open Access Article. Published on 03 Feabhra 2023. Downloaded on 28/04/2026 00:38:03.
This article is licensed under a Creative Commons Attribution-NonCommercial 3.0 Unported Licence.

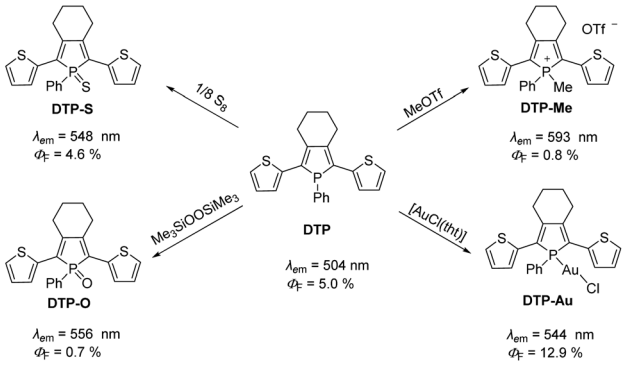

Scheme 1 Chemical modification of dithienyl-phosphole (DTP) and changes in photophysical properties.[21,24]

incorporating phospholes in such π systems are based on their electronic structure. In general, a modification of the environment around the phosphorus atom leads to a reduction of the gap energies of the highest energy occupied molecular orbital (HOMO) and the lowest energy unoccupied molecular orbital (LUMO) resulting in lower energies for the emitted photons.[24] Several options for the chemical modification of phospholes have already been described in the literature. Besides alkylation[28] or oxidation with chalcogens (O, S, and Se),[29–31] the electronic structure of the phosphole framework can be changed by complex formation with various metals.[32–35]

In this work, we present a powerful synthetic strategy for selectively converting phosphole oxides by reaction with sulfonyl isocyanates into the corresponding sulfonylimino phospholes, which showed tunable phosphole-based AIE with high Φ_F in the solid state.

Results and discussion

Only a few reactions in which cyclic phosphane oxides are selectively converted into their phosphane imines have already been reported in the literature.[36,37] Herein, we investigated the reaction of four structurally different phosphole oxides **1–4** (Scheme 2) with chlorosulfonyl isocyanate (**5a**, CSI) and *p*-toluenesulfonyl isocyanate (**5b**, TSI). CSI **5a** is the most reactive isocyanate known.[38] In addition to the well-known cycloadditions, a wide variety of nucleophilic addition and substitution reactions are possible, making CSI a powerful reagent.[39]

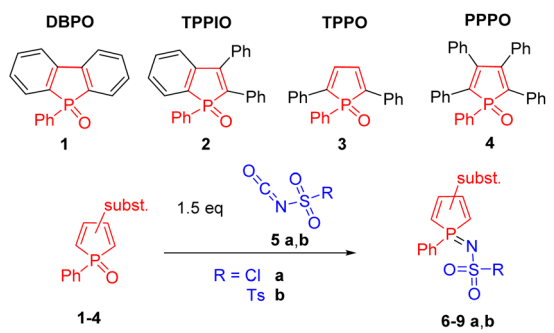

Scheme 2 Synthesis of sulfonylimino phospholes **6–9 a,b**.

When phosphole oxides **1–4** were treated with a solution of **5a**, we could observe a specific reaction behavior. **5a** undergoes a highly chemoselective reaction with phosphole oxides **1–4** resulting in chlorosulfonylimino phospholes **6a–9a**, where the reaction conditions strongly depend on the structure of the phosphole oxide used (Table 1). DBPO **1** exhibits the highest reactivity due to its planar structure and the good accessibility of the P=O double bond. Complete conversion is achieved after 2 h at −30 °C. In contrast, TPPO **3** and PPPO **4** show the lowest reactivity as a result of the phenyl rings in the α position to the phosphorus atom and the stronger steric hindrance. In these cases, complete conversion was observed up to 24 h at RT. All the products were isolated *via* recrystallization giving **6a–9a** in 90–98% yields. The ^{31}P NMR signals of the compounds **6a–9a** are shifted to a higher field by about 12–14 ppm compared to the corresponding phosphole oxides **1–4**, allowing the reaction progress to be easily monitored by ^{31}P NMR spectroscopy. Phospholes **6a–9a** are moisture-insensitive in the crystalline form but show slow hydrolysis and substitution reactions in the presence of nucleophiles in solution. *p*-Tolylsulfonylimino phospholes **6b–9b** can be obtained when TSI **5b** is employed; nonetheless, higher reaction temperatures are required due to the lower reactivity of TSI **5b** compared to CSI **5a**. Phospholes **6b–9b** were formed highly chemoselectively in good yields (80–97%). Here, the phosphole oxides TPPO **3** and PPPO **4** required temperatures up to 85 °C, which are significantly higher than in the case of DBPO **1**. Derivatives **6b–9b** are moisture and air stable and can be purified by flash chromatography in addition to recrystallization. The exchange of the chlorine group by a tosyl moiety leads to a higher electron density at the phosphorus atom, which is shown by a low field shift of 4 to 5 ppm in the ^{31}P NMR spectrum. Even though a few examples of sulfonylimino phospholes have already been reported in the literature, they were obtained by the reaction of phospholes with sulfonyl azides[40] or chloramine T.[41,42] The advantage of our approach is the selective and facile synthesis of iminophospholes starting from air-stable and easily isolable phosphole oxides **1–4**.

To obtain a deeper insight into the possible reaction mechanism of the formation of sulfonylimino phospholes, computational studies using DBPO **1** and chlorosulfonyl isocyanate **5a** were performed at the B3LYP-D3(BJ)/TZP level of

Table 1 Conditions and characteristics for the synthesis of sulfonylimino phospholes **6–9 a,b**

Entry	Solvent	Time [h]	Temp. [°C]	Yield[a] %	^{31}P NMR[b] [ppm]
6a	CH_2Cl_2	2	−30	92	21.2
7a	CH_2Cl_2	3	0	90	25.8
8a	CH_2Cl_2	24	RT	91	28.0
9a	CH_2Cl_2	24	RT	98	31.0
6b	CH_2Cl_2	14	40	80	17.1
7b	Toluene	14	70	97	21.0
8b	Toluene	14	85	82	22.1
9b	Toluene	14	85	85	26.1

[a] Isolated yield. [b] Measured in $CDCl_3$.

© 2023 The Author(s). Published by the Royal Society of Chemistry

Open Access Article. Published on 03 Feabhra 2023. Downloaded on 28/04/2026 00:38:03.
This article is licensed under a Creative Commons Attribution-NonCommercial 3.0 Unported Licence.

theory[43] using ADF.2018.107.[44,45] Transition states were located by employing the Climbing Image Nudged Elastic Band (CI-NEB) method[46] starting from the relaxed ground state structures of the reactants (Chapter 5, ESI†).

Fig. 2 shows the relative Gibbs free energy profile of the reaction regarding the starting materials (SM). Theoretical calculations indicated that the phosphole sulfonylimination reaction proceeded *via* an addition–elimination mechanism and could be considered a formal [2 + 2] cycloaddition. First, the oxygen atom of the P=O double bond attacks the carbon atom of the isocyanate. In the resulting ionic intermediate (Int), the negatively charged nitrogen atom attacks the phosphorus atom of the phosphole framework, yielding the corresponding sulfonylimino phosphole after the elimination of CO_2. In the exergonic reaction, an energy of 67.3 kJ mol^{-1} is released and the driving forces are the generation of a C=O double bond, the elimination of CO_2, and the formation of a resonance-stabilized P–N–S moiety. Interestingly, acyclic phosphane oxides, such as triphenylphosphane oxide, cannot be converted to the corresponding sulfonylimines by CSI **5a**. The reason is the more stable and sterically protected P=O double bond compared to phosphole oxides. However, TSI **5b** exhibits higher thermal stability, which allowed the conversion of triphenylphosphane oxide to tosylimino phosphane at high temperatures and long reaction times (Fig. S1.2, ESI†).

Sulfonylimino phospholes are characterized by excellent crystallization properties, readily furnishing single crystals suitable for X-ray diffractometric structure analysis by common crystallization methods (Table 2). The P=N double bonds (1.603–1.613 Å) in phospholes **6a–9a** (Fig. 3) agree with the calculated (1.61 Å) and reported values.[47] Interestingly, the S1–N1 bond lengths are in a range of 1.550 to 1.561 Å and indicate double bond character. This observation suggests delocalization in the P–N–S moiety, which is stabilized by the neighboring electron-withdrawing groups. A comparable delocalized P–N–S unit has already been reported by Dehnicke *et al.* for sulfonylimino phosphoranes.[47] The bond length of the characteristic S–Cl bond is in a range of 2.078 to 2.080 Å and slightly longer than in comparable compounds.[47] The tolyl

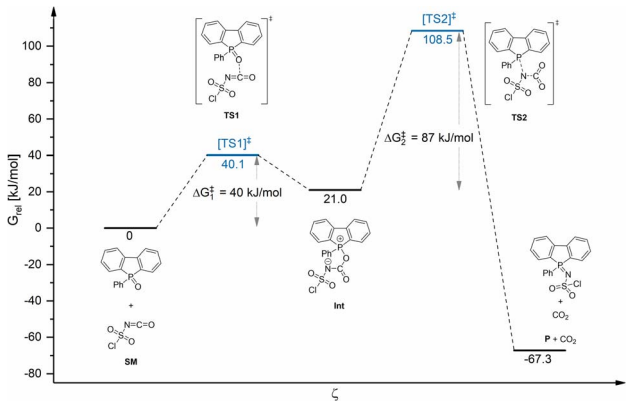

Fig. 2 Relative Gibbs free energy profile of the reaction with respect to the starting materials.

Table 2 Selected bond lengths [Å] and angles [°] of phospholes **6a–9a**

	6a	7a	8a	9a
P1–C1	1.790(2)	1.791(2)	1.816(5)	1.798(2)
P1–N1	1.603(1)	1.610(2)	1.609(4)	1.613(1)
N1–S1	1.550(1)	1.548(2)	1.557(4)	1.561(1)
S1–Cl1	2.0778(5)	2.0803(9)	2.079(2)	2.077(1)
P1–N1–S1	127.13(8)	123.2(1)	122.3(3)	125.61(8)
C1–P1–C4	93.61(7)	94.0(1)	94.8(2)	94.69(7)

derivatives **6b–9b** (Fig. 4) show structural differences compared to their chlorine derivatives **6a–9a**. The P=N bonds are shorter by 0.01 to 0.04 Å and the S–N bonds are longer by 0.02 to 0.04 Å, resulting in almost equal S–N and P–N bond lengths.

The interesting P–N–S bonding mode of sulfonylimino phospholes is possibly the cause of the high kinetic stability of this class of compounds.[48] Compared to the chlorine substituent, the tolyl group does not have any electron-withdrawing properties, which leads to a stronger S–N single bond character and reduced delocalization (Table 3).[49] For the annelated derivatives **6b** and **7b**, a significant increase of the P–N–S bond angle is observed compared to the corresponding chlorine derivatives, whereas a decrease is observed for the phospholes with exocyclic substituents **8b** and **9b**. This is due to intramolecular π interactions between the tosyl group and the fused rings, which leads to an increased tension of the P–N–S linker and increase of the bond angle. In **8b** and **9b**, the intramolecular π interaction takes place between the tosyl group and the exocyclic phenyl rings in the α position of the phospholes. In addition, the derivatives **6b–8b** show a decrease in the C1–P1–C4 bond angle by 0.5 to 1.0°. Significant intermolecular π–π stacking could only be observed in compounds **6b**, **8a**, and **8b** (see Chapter 2, ESI†).

Phosphole-based conjugated π systems are characterized by remarkable photophysical properties. Therefore, in-depth

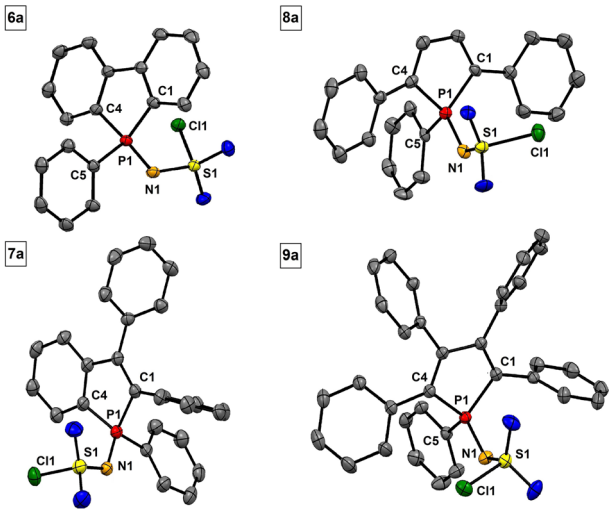

Fig. 3 Molecular structures of **6a**, **7a**, **8a**, and **9a**. Thermal displacement ellipsoids shown at 50% probability. Hydrogen atoms have been omitted for clarity.

Open Access Article. Published on 03 Feabhra 2023. Downloaded on 28/04/2026 00:38:03.
This article is licensed under a Creative Commons Attribution-NonCommercial 3.0 Unported Licence.

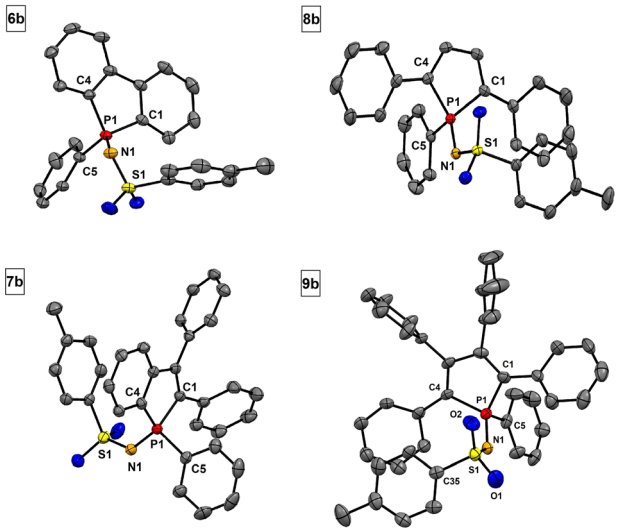

Fig. 4 Molecular structures of **6b**, **7b**, **8b** and **9b**. Thermal displacement ellipsoids shown at 50% probability. Hydrogen atoms have been omitted for clarity.

Table 3 Selected bond lengths [Å] and angles [°] of phospholes **6b–9b**

	6b	7b	8b	9b
P1–C1	1.792(1)	1.807(2)	1.814(1)	1.802(8)[a]
P1–N1	1.591(1)	1.587(2)	1.595(1)	1.585(6)[a]
N1–S1	1.582(1)	1.586(2)	1.591(1)	1.591(6)[a]
P1–N1–S1	128.99(8)	129.5(1)	121.73(6)	123.6(4)[a]
C1–P1–C4	93.03(7)	93.0(1)	94.18(6)	94.4(4)[a]

[a] Average bond lengths and bond angles of the three molecules.

photophysical studies of phospholes **6–9 a,b** were carried out to understand the influence of the new modification method on the optical properties. Relating to this, photoluminescence spectra and excited state lifetimes (τ_{av_amp}), as well as Φ_F in fluid solution at RT, in a frozen glassy matrix at 77 K and in the solid state were measured (Table 4). In general, we observed that all time-resolved photoluminescence measurements yield biexponential decays, due to the coexistence of different conformers; thus, amplitude-weighted average lifetimes were used to estimate deactivation rate constants.[50] It became apparent that the chemical modification of the phosphorus atom strongly influences the optical properties. All derivatives show that the transformation from oxides **1–4** into sulfonylimines **6–9 a,b** leads to a bathochromic shift of the absorption (λ_{ex}) and emission maxima (λ_{em}) (Fig. 5). Similar observations were already reported by Matano *et al.*[40]

The shifts in the UV/vis absorption spectra are in the range of 8–18 nm for the chlorine derivatives **6a–9a** and 2–13 nm for the tosyl derivatives **6b–9b**. However, this effect is even more evident in the steady-state fluorescence spectra, wherein the emission maxima show changes in a range of 21–48 nm for **6a–9a** and 14–29 nm for **6b–9b**, if compared with their oxide precursors. The largest bathochromic shift is observed in **8a**, which shows a difference of 47 nm compared to the oxide **3** ($\lambda_{em} = 508$ nm). The bathochromic shift can be explained by the fact that sulfonylimino phospholes have a more extended π system than their corresponding oxides. The transformation leads to a reduction of the HOMO–LUMO energy gaps resulting in longer wavelength photons (Fig. S5.1, ESI†). Herein, the chlorine derivatives **6a–9a** show the highest bathochromic shift due to the electron-withdrawing properties of the sulfonyl

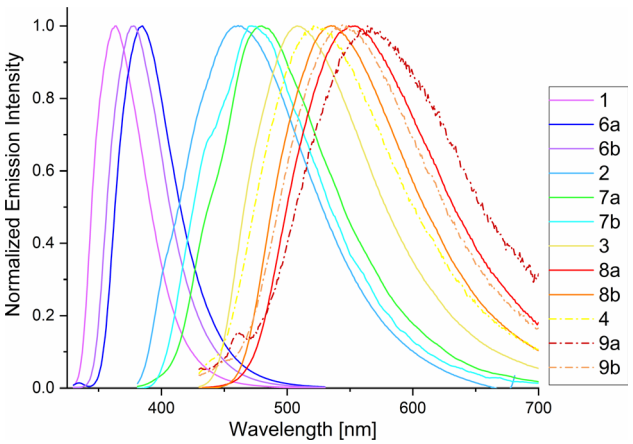

Fig. 5 Photoluminescence spectra of **1–4** and **6–9 a,b** in MeCN at RT (for λ_{ex}, see Chapter 4, ESI†).

Table 4 Photophysical properties of **6–9 a,b** in MeCN solutions at RT and frozen glassy matrices of butyronitrile at 77 K

Compound	λ_{ex}[a] [nm]	ε[a] [10^3 mol^{-1} dm^3 cm^{-1}]	λ_{em}[a] [nm]	$\tau_{av_amp\ (sol,\ RT)}$[a,b] [ns]	$\tau_{av_amp(77\ K)}$[b,c] [ns]	$\Phi_{F(IS)}$[a,d] [±2%]	$\Phi_{F(SR)}$[a,e] [±2%]	$\Phi_{F(77\ K)}$[c,d] [±2%]
6a	335	1.59	385	2.33 ± 0.01	3.82 ± 0.06	16	15	98
6b	330	1.69	378	12.57 ± 0.04	13.7 ± 0.1	10	12	77
7a	357	5.80	480	0.84 ± 0.01	12.21 ± 0.08	5	4	85
7b	353	4.30	472	0.74 ± 0.01	12.16 ± 0.04	5	10	98
8a	410	12.60	555	0.104 ± 0.002	6.46 ± 0.04	<2	<2	78
8b	405	16.30	537	0.407 ± 0.001	7.63 ± 0.02	3	4	62
9a	405	5.20	558	n. d.[f]	11.1 ± 0.1	<2	<2	83
9b	398	5.00	547	3.54 ± 0.08	14.9 ± 0.1	<2	<2	89

[a] Measured in MeCN solutions at RT. [b] Amplitude-weighted average lifetimes (τ_{av_amp}).[50] [c] Frozen glassy matrices of butyronitrile at 77 K. [d] Absolute $\Phi_{F(IS)}$ was obtained using a calibrated integrating sphere. [e] $\Phi_{F(SR)}$ was determined by a comparative approach using 1,6-diphenyl-1,3,5-hexatriene (DPHT) in cyclohexane as the standard reference ($\Phi_{F(RT)} = 0.78$). [f] Not detectable due to weak fluorescence.

© 2023 The Author(s). Published by the Royal Society of Chemistry

Open Access Article. Published on 03 Feabhra 2023. Downloaded on 28/04/2026 00:38:03.
This article is licensed under a Creative Commons Attribution-NonCommercial 3.0 Unported Licence.

chloride group. The respective fluorescence quantum yields in fluid solutions at RT ($\Phi_{F(IS)}$) were obtained in acetonitrile using a calibrated integrating sphere system and showed a strong dependence on the molecular structure. These $\Phi_{F(IS)}$ values were additionally confirmed by a relative method and the use of DPHT as a standard reference.

In MeCN solutions at RT, dibenzophosphole derivatives **6a** and **6b** have Φ_F values of 16% and 10%, respectively, which are significantly higher than that of the corresponding DBPO **1** (Φ_F = 4.2%).[22] Similar observations were made with the phosphindole derivatives **7a** and **7b**. The Φ_F values for both derivatives are 5%, which is considerably higher than that of their precursor TPPIO **2** (Φ_F = 1.2%).[12] The higher k_{nr} values of compounds **7a-b** (if compared with **6a-b**) explain their lower quantum yields, which can be attributed to their reduced rigidity. The lowest Φ_F values are shown by derivatives **8** and **9**. This behavior can be explained by comparison of the corresponding rates, where higher radiationless constants k_{nr} were observed for derivatives **8** and **9** (Table S4.1, ESI†). This illustrates that these compounds, as well as the corresponding oxides **3** and **4**, are weak emitters in solution with Φ_F values < 2-3%. For these molecules, high rates of vibronic radiationless relaxation can be inferred, due to the rotation of the exocyclic phenyl rings, which favors a non-radiative decay and ultimately leads to a decrease in the emission intensity. **6a** and **6b** have significantly more rigid and planar configurations and thus show a stronger emission in solution. The rotation of the exocyclic phenyl rings and non-radiative decays can be hindered in frozen matrices, meaning that the emission can be strongly enhanced.[51] For this purpose, the compounds were dissolved in butyronitrile and cooled down to 77 K. All derivatives show a significant increase in emission intensity at 77 K; this can be confirmed by $\Phi_{F(77\ K)}$, whose values are in a range of 62–98%. Moreover, the excited state lifetimes ($\tau_{av_amp(77\ K)}$) are longer than at RT. **8a** has a $\tau_{av_amp(77\ K)}$ of 6.46 ns, which means a lifetime extension of more than 60 times compared to RT. Except for **6a**, the k_r values for all compounds are comparable to RT when cooling down to 77 K. However, an important decrease of until two orders of magnitude in the k_{nr} values is observed for all derivatives in frozen glassy matrices, if compared with RT. This behavior is explained by the lack of vibronic radiationless relaxation in the frozen matrices. Interestingly, derivatives **8** and **9**, which are those with the largest number of phenyl substituents, are the ones with the most significant drop in the k_{nr} value. These results are in agreement with the detected $\Phi_{F(77\ K)}$ and $\tau_{av_amp(77\ K)}$.

AIEgens are characterized by weak fluorescence in solution. By adding a solvent in which the compound is not soluble, they aggregate. The resulting intermolecular interactions restrict the rotational freedom of the exocyclic rotor units, which leads to a significant increase in fluorescence intensity. We have shown this typical AIE behavior for the examples **8b** and **9b** in Fig. 6. The MeCN solutions of compounds **8b** and **9b** show no (**9b**) or weak (**8b**) fluorescence (Fig. 6B). When the water content is increased, a drastic increase in emission intensity is observed at about 80% water content, which illustrates the AIE nature of this novel class of compounds.

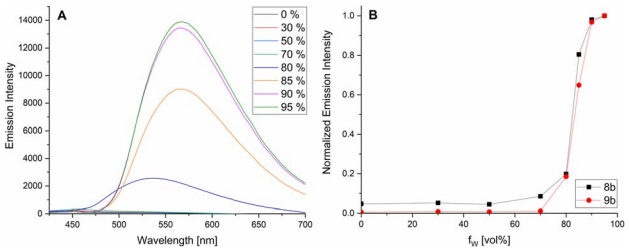

Fig. 6 Photoluminescence spectra of **9b** in different MeCN/water mixtures (λ_{ex} = 398 nm) (A) and emission intensity of **8b** and **9b** in MeCN/water for increasing water content (f_w) (B).

Despite sulfonylimino phospholes showing weak emission in solution, they are strong emitters in the solid state (Fig. 7). The locations of the emission maxima are comparable to those in solution (Table 5). Exceptions are represented by the dibenzophosphole derivatives **6a** and **6b**, which show a strong bathochromic shift of 29–31 nm that can be attributed to the fact that planar molecular structures are capable of forming stronger interactions by π–π stacking in the solid state.[52] The Φ_F values in the solid state ($\Phi_{F(solid)}$) as well as τ_{av_amp} show characteristic differences between chlorine and tosyl derivates. **9b** has a $\Phi_{F(solid)}$ value of 75%, which is more than two-fold higher than that of the corresponding oxide PPPO **4** ($\Phi_{F(solid)}$ = 36%), whereas **9a** shows less emission with a $\Phi_{F(solid)}$ of 10%. Furthermore, **7b** shows intense blue fluorescence at 479 nm and a $\Phi_{F(solid)}$ of 82%, which represents a significant increase if compared to TPPIO **2** ($\Phi_{F(solid)}$ = 72%). Interestingly, for all the compounds studied, a trend was observed for the tosyl derivatives **6b–9b**, which have larger $\Phi_{F(solid)}$ and longer τ in the solid state than the comparable Cl derivatives **6a–9a**. These differences in τ_{av_amp} and $\Phi_{F(solid)}$ can be explained by analyzing and comparing the average radiative decay rate constants (k_r) and the corresponding non-radiative decay rate constants (k_{nr}).

In **6a–9a**, larger k_{nr} than k_r values are observed. This is clearly demonstrated by phospholes **8a** and **9a**, which have a k_{nr} of $36 \times 10^7\ s^{-1}$ and k_r of $8.0 \times 10^7\ s^{-1}$ and $3.8 \times 10^7\ s^{-1}$, respectively (Fig. 8). We could observe in the crystal structures that the Cl substituent of the sulfonyl group has no contact with neighboring molecules and can undergo rotation and vibration, leading to higher rates of radiationless vibrational relaxation,

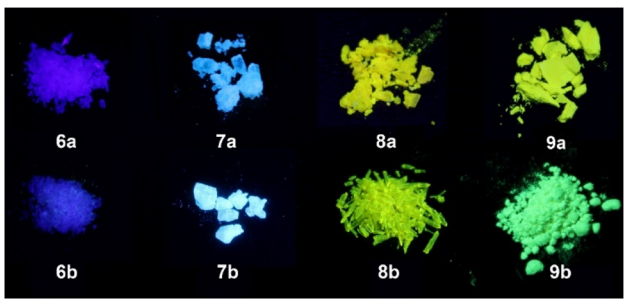

Fig. 7 Solid-state fluorescence of phospholes **6–9** under irradiation of UV light (395 nm).

Open Access Article. Published on 03 Feabhra 2023. Downloaded on 28/04/2026 00:38:03.
This article is licensed under a Creative Commons Attribution-NonCommercial 3.0 Unported Licence.

Table 5 Photophysical properties of **6–9 a,b** in the solid state

Compound	λ_{em} [a] [nm]	τ_{av_amp} [b] [ns]	$\Phi_{F(solid)}$ [c] [± 2%]
6a	417	8.4 ± 0.4	34
6b	407	14.2 ± 0.3	54
7a	491	4.4 ± 0.1	46
7b	479	8.5 ± 0.5	82
8a	557	2.3 ± 0.1	18
8b	548	9.2 ± 0.5	55
9a	555	2.5 ± 0.1	10
9b	528	8.1 ± 0.1	75

[a] Solid state at RT. [b] Amplitude-weighted average lifetimes at RT. [c] Absolute Φ_F of solids at RT was obtained using a calibrated integrating sphere with a suitable sample holder.

and thus, an increased radiationless decay rate. Moreover, C_{aryl}–H···Cl interactions occur in **6a** and **7a**, resulting in increased rigidity, relatively low k_{nr} values and moderate $\Phi_{F(solid)}$ of 34 and 46%, respectively (additional details are given in the ESI†). On the other hand, there are multiple C_{aryl}–H···π and S=O···H interactions in **6b–9b** between the tosyl group and neighboring molecules. The resulting restriction of rotations and motions due to the fixation of the substituent is clearly reflected in the lower k_{nr} values.

Also, additional intramolecular π–π interactions between the tosyl group and the phoshindole framework or the exocyclic phenyl rings in the α position can be noticed (Fig. 9). This type of through-space conjugation has been invoked to explain the enhanced photophysical properties by increased rigidity.[53–56] The distances of the intramolecular π stacking are in the range of 3.219–3.501 Å, indicating strong interactions and agreeing with the observations of Tang *et al.*[57] Except for **7a-b** and **9b** having the highest radiative rate constants, the k_{nr} values are generally comparable for all compounds in solid phases.

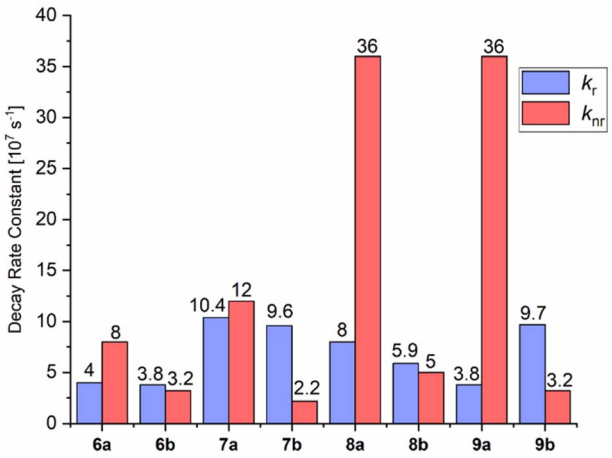

Fig. 8 Radiative (k_r) and non-radiative (k_{nr}) decay rate constants of compounds **6–9** in the solid state. The decay rate constants are determined according to $k_r = 1/\tau_{av_amp} = \Phi_F/\tau_{av_amp}$ and $k_{nr} = 1 - \Phi_F/\tau_{av_amp}$ by using amplitude-weighted average lifetimes, according to Engelborghs *et al.*[50] The uncertainty analysis is not presented in this diagram for clarity (for k_r and k_{nr} in MeCN solutions at RT and a frozen glassy matrix in butyronitrile at 77 K, see Chapter 4 in the ESI†).

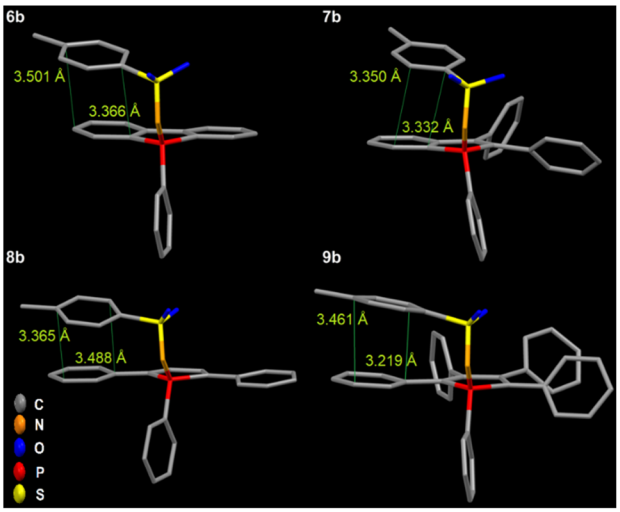

Fig. 9 Intramolecular π–π interaction with the tosyl group in **6b–9b** leads to through-space conjugation, additional restriction of motions, and increased rigidity.

In general, the derivatisation of phosphole oxides with sulfonyl isocyanates results in a bathochromic shift of the absorption and emission maxima. All synthesized phospholes **6–9** show a weaker emission in solution, whereas **6a,b**, and **7a,b** have higher Φ_F values than the corresponding oxides **1** and **2**. Due to the different restrictions in motions and intramolecular interactions, tosyl derivatives **6b–9b** have significantly higher $\Phi_{F(solid)}$ values than chlorine derivatives **6a–9a.** The high density of rotovibrational states make oxides **3-4** and derivatives **8-9** weak emitters in fluid solutions. This highlights the importance of the reaction of phosphole oxides with TSI **5b** as a promising derivatisation method for the synthesis of high-emissive phosphole-based AIEgens.

Conclusion

A facile synthetic strategy for selectively converting phosphole oxides **1–4** into their corresponding sulfonylimines **6–9 a,b** by using sulfonyl isocyanates **5a,b** is reported. The reaction is characterized by high chemoselectivity and excellent yields. Theoretical calculations suggest an addition–elimination mechanism and show that this reaction method is particularly suitable for phosphole oxides. In addition to X-ray structure analysis, the photophysical properties of the phospholes **6–9 a,b** were studied under different conditions, namely in solution, frozen glassy matrices, and solid state. In solution, all compounds show a bathochromic shift of absorption and emission maxima compared to the phosphole oxides **1–4**, but low $\Phi_{F(IS)}$ values were observed. At 77 K in glassy matrices, however, the Φ_F values were significantly improved. The novel compounds are characterized by strong fluorescence in the solid state, although there are significant differences in quantum yields and lifetimes between chloride **6a–9a** and tosyl derivates **6b–9b.** In general, a trend towards considerably higher $\Phi_{F(solid)}$ values and longer τ for tosyl derivatives **6b–9b** is

© 2023 The Author(s). Published by the Royal Society of Chemistry

Open Access Article. Published on 03 Feabhra 2023. Downloaded on 28/04/2026 00:38:03.
This article is licensed under a Creative Commons Attribution-NonCommercial 3.0 Unported Licence.

observed, due to better restriction of intramolecular rotations and vibrations in the solid state. Intriguingly, the transformation of phosphole oxides into their tosylimines significantly increased the quantum yield. These observations show that derivatisation with TSI **5b** is an essential and facile synthetic strategy for the preparation of highly emissive phosphole-based luminophores and its potential will now be investigated further.

Data availability

All experimental procedures, spectroscopic data, photophysical properties, information on the theoretical calculations and crystallographic data can be found in the ESI.†

Author contributions

N. K. performed the experimental work and wrote the original draft. Y. G.-L., C. L. and F. Y. analyzed the photophysical properties. P. L. performed single crystal X-ray analysis and interpreted the structural data. M. L. performed the DFT calculations. E. H.-H. and C. A. S. supervised the project. All authors have corrected the final manuscript. All authors have read and approved the final version.

Conflicts of interest

There are no conflicts to declare.

Acknowledgements

M. L. is grateful for a doctoral fellowship provided by the Deutsche Bundesstiftung Umwelt. We thank Prof. Dr C. Schneider for providing the computational infrastructure for DFT calculations. C. A. S. gratefully acknowledges the generous financial support for the acquisition of an "Integrated Confocal Luminescence Spectrometer with Spatiotemporal Resolution and Multiphoton Excitation" (DFG/Land NRW: INST 211/915-1 FUGG; DFG EXC1003: "Berufungsmittel"). We thank Prof. Dr B. Abel for providing access to the fluorescence lifetime image microscope for the kinetical fluorescence studies.

References

1 J. Luo, Z. Xie, J. W. Y. Lam, L. Cheng, H. Chen, C. Qiu, H. S. Kwok, X. Zhan, Y. Liu, D. Zhu and B. Z. Tang, *Chem. Commun.*, 2001, 1740–1741.
2 J. Mei, N. L. C. Leung, R. T. K. Kwok, J. W. Y. Lam and B. Z. Tang, *Chem. Rev.*, 2015, **115**, 11718–11940.
3 B. Liu and B. Z. Tang, *Chem. –J. Mater. Chem. B Asian J.*, 2019, **14**, 672–673.
4 R. Zhan, Y. Pan, P. N. Manghnani and B. Liu, *Macromol. Biosci.*, 2017, **17**, 1600433.
5 G. Feng and B. Liu, *Acc. Chem. Res.*, 2018, **51**, 1404–1414.
6 X. Zhang, X. Zhang, L. Tao, Z. Chi, J. Xu and Y. Wei, *J. Mater. Chem. B*, 2014, **2**, 4398–4414.
7 J. Mei, Y. Hong, J. W. Y. Lam, A. Qin, Y. Tang and B. Z. Tang, *Adv. Mater.*, 2014, **26**, 5429–5479.
8 L. Chen, C. Zhang, G. Lin, H. Nie, W. Luo, Z. Zhuang, S. Ding, R. Hu, S.-J. Su, F. Huang, A. Qin, Z. Zhao and B. Z. Tang, *J. Mater. Chem. C*, 2016, **4**, 2775–2783.
9 Z. Zhao, H. Zhang, J. W. Y. Lam and B. Z. Tang, *Angew. Chem., Int. Ed.*, 2020, **59**, 9888–9907.
10 Z. Zhao, J. W. Y. Lam and B. Z. Tang, *J. Mater. Chem.*, 2012, **22**, 23726–23740.
11 G. Yu, S. Yin, Y. Liu, J. Chen, X. Xu, X. Sun, D. Ma, X. Zhan, Q. Peng, Z. Shuai, B. Tang, D. Zhu, W. Fang and Y. Luo, *J. Am. Chem. Soc.*, 2005, **127**, 6335–6346.
12 F. Bu, E. Wang, Q. Peng, R. Hu, A. Qin, Z. Zhao and B. Z. Tang, *Chem. – Eur. J.*, 2015, **21**, 4440–4449.
13 J. Chen, C. C. W. Law, J. W. Y. Lam, Y. Dong, S. M. F. Lo, I. D. Williams, D. Zhu and B. Z. Tang, *Chem. Mater.*, 2003, **15**, 1535–1546.
14 Y. Hong, J. W. Y. Lam and B. Z. Tang, *Chem. Commun.*, 2009, 4332–4353.
15 Z. Zhao, S. Chen, J. W. Y. Lam, C. K. W. Jim, C. Y. K. Chan, Z. Wang, P. Lu, C. Deng, H. S. Kwok, Y. Ma and B. Z. Tang, *J. Phys. Chem. C*, 2010, **114**, 7963–7972.
16 M. Chen, L. Li, H. Nie, J. Tong, L. Yan, B. Xu, J. Z. Sun, W. Tian, Z. Zhao, A. Qin and B. Z. Tang, *Chem. Sci.*, 2015, **6**, 1932–1937.
17 Y. Ren and T. Baumgartner, *Dalton Trans.*, 2012, **41**, 7792–7800.
18 J. C.-H. Chan, W. H. Lam, H.-L. Wong, W.-T. Wong and V. W.-W. Yam, *Angew. Chem., Int. Ed.*, 2013, **52**, 11504–11508.
19 M. P. Duffy, W. Delaunay, P.-A. Bouit and M. Hissler, *Chem. Soc. Rev.*, 2016, **45**, 5296–5310.
20 D. Joly, D. Tondelier, V. Deborde, B. Geffroy, M. Hissler and R. Réau, *New J. Chem.*, 2010, **34**, 1603–1611.
21 C. Hay, M. Hissler, C. Fischmeister, J. Rault-Berthelot, L. Toupet, L. Nyulászi and R. Réau, *Chem. – Eur. J.*, 2001, **7**, 4222–4236.
22 H.-C. Su, O. Fadhel, C.-J. Yang, T.-Y. Cho, C. Fave, M. Hissler, C.-C. Wu and R. Réau, *J. Am. Chem. Soc.*, 2006, **128**, 983–995.
23 C. Hay, C. Fave, M. Hissler, J. Rault-Berthelot and R. Réau, *Org. Lett.*, 2003, **5**, 3467–3470.
24 J. Crassous and R. Réau, *Dalton Trans.*, 2008, 6865–6876.
25 F. Mathey, *Chem. Rev.*, 1988, **88**, 429–453.
26 P. R. Schleyer, H. Jiao, B. Goldfuss and P. K. Freeman, *Angew. Chem., Int. Ed. Engl.*, 1995, **34**, 337–340.
27 A. Dransfeld, L. Nyulászi and P. R. Schleyer, *Inorg. Chem.*, 1998, **37**, 4413–4420.
28 Y. Ren, J. Gao, A. K. Hailey, T. Baumgartner and Y.-L. Loo, *Chem. Mater.*, 2016, **28**, 8407–8414.
29 D. Klintuch, A. Kirchmeier, C. Bruhn and R. Pietschnig, *Dyes Pigm.*, 2020, **180**, 108443.
30 R. Kabe, V. M. Lynch and P. Jr Anzenbacher, *CrystEngComm*, 2011, **13**, 5423–5427.
31 M. Matsumura, M. Yamada, A. Muranaka, M. Kanai, N. Kakusawa, D. Hashizume, M. Uchiyama and S. Yasuike, *Beilstein J. Org. Chem.*, 2017, **13**, 2304–2309.

Open Access Article. Published on 03 Feabhra 2023. Downloaded on 28/04/2026 00:38:03.
This article is licensed under a Creative Commons Attribution-NonCommercial 3.0 Unported Licence.

32 E. Takacs, A. Escande, N. Vanthuyne, C. Roussel, C. Lescop, E. Guinard, C. Latouche, A. Boucekkine, J. Crassous, R. Réau and M. Hissler, *Chem. Commun.*, 2012, **48**, 6705–6707.
33 M. Hissler, C. Lescop and R. Réau, *C. R. Chim.*, 2008, **11**, 628–640.
34 K. Fourmy, D. H. Nguyen, O. Dechy-Cabaret and M. Gouygou, *Catal. Sci. Technol.*, 2015, **5**, 4289–4323.
35 O. Fadhel, D. Szieberth, V. Deborde, C. Lescop, L. Nyulászi, M. Hissler and R. Réau, *Chem. – Eur. J.*, 2009, **15**, 4914–4924.
36 H. Hoffmann, H. Förster and G. Tor-Poghossian, *Monatsh. Chem.*, 1969, **100**, 311–315.
37 C. R. Hall and D. J. H. Smith, *Tetrahedron Lett.*, 1974, **15**, 1693–1696.
38 Y. Chemam, Z. Aouf, A. Amira, H. K'tir, H. Bentoumi, R. Ghodbane, R. Zerrouki and N.-E. Aouf, *Phosphorus, Sulfur Silicon Relat. Elem.*, 2022, **197**, 777–787.
39 J. K. Rasmussen and A. Hassner, *Chem. Rev.*, 1976, **76**, 389–408.
40 Y. Matano, H. Ohkubo, Y. Honsho, A. Saito, S. Seki and H. Imahori, *Org. Lett.*, 2013, **15**, 932–935.
41 U. V. Monkowius, S. Nogai and H. Schmidbaur, *Dalton Trans.*, 2004, 1610–1617.
42 G. Wittig and A. Maercker, *Chem. Ber.*, 1964, **97**, 747–768.
43 G. te Velde, F. M. Bickelhaupt, E. J. Baerends, C. Fonseca Guerra, S. J. A. van Gisbergen, J. G. Snijders and T. Ziegler, *J. Comput. Chem.*, 2001, **22**, 931–967.
44 M. Ernzerhof and G. E. Scuseria, *J. Chem. Phys.*, 1999, **110**, 5029–5036.
45 S. Grimme, *J. Comput. Chem.*, 2004, **25**, 1463–1473.
46 G. Henkelman, B. P. Uberuaga and H. Jónsson, *J. Chem. Phys.*, 2000, **113**, 9901–9904.
47 H. Folkerts, D. Nußhär, F. Weller, K. Dehnicke, J. Magull and W. Hiller, *Z. Anorg. Allg. Chem.*, 1994, **620**, 1986–1991.
48 E. Böhm, K. Dehnicke, J. Beck, W. Hiller, J. Strähle, A. Maurer and D. Fenske, *Z. Naturforsch., B: J. Chem. Sci.*, 1988, **43**, 138–148.
49 A. F. Cameron, N. J. Hair and D. G. Morris, *Acta Crystallogr., Sect. B: Struct. Crystallogr. Cryst. Chem.*, 1974, **30**, 221–225.
50 A. Sillen and Y. Engelborghs, *Photochem. Photobiol.*, 1998, **67**, 475–486.
51 G. Tan, I. Maisuls, F. Strieth-Kalthoff, X. Zhang, C. Daniliuc, C. A. Strassert and F. Glorius, *Adv. Sci.*, 2021, **8**, 2101814.
52 M. Yamaguchi, S. Ito, A. Hirose, K. Tanaka and Y. Chujo, *Mater. Chem. Front.*, 2017, **1**, 1573–1579.
53 J. Li, P. Shen, Z. Zhao and B. Z. Tang, *CCS Chem.*, 2019, **1**, 181–196.
54 W. Luo, H. Nie, B. He, Z. Zhao, Q. Peng and B. Z. Tang, *Chem. – Eur. J.*, 2017, **23**, 18041–18048.
55 H. Puntscher, P. Kautny, B. Stöger, A. Tissot, C. Hametner, H. R. Hagemann, J. Fröhlich, T. Baumgartner and D. Lumpi, *RSC Adv.*, 2015, **5**, 93797–93807.
56 M. Yu, R. Huang, J. Guo, Z. Zhao and B. Z. Tang, *PhotoniX*, 2020, **1**, 11.
57 T. Han, H. Deng, Z. Qiu, Z. Zhao, H. Zhang, H. Zou, N. L. C. Leung, G. Shan, M. R. J. Elsegood, J. W. Y. Lam and B. Z. Tang, *J. Am. Chem. Soc.*, 2018, **140**, 5588–5598.

© 2023 The Author(s). Published by the Royal Society of Chemistry